



Epitope Classification and RBD Binding Properties of Neutralizing Antibodies Against SARS-CoV-2 Variants of Concern

Ashlesha Deshpande¹, Bethany D. Harris¹, Luis Martinez-Sobrido², James J. Kobie³ and Mark R. Walter^{1*}

¹ Department of Microbiology, University of Alabama at Birmingham, Birmingham, AL, United States, ² Disease Intervention & Prevention Program, Texas Biomedical Research Institute, San Antonio, TX, United States, ³ Department of Medicine, Division of Infectious Diseases, University of Alabama at Birmingham, Birmingham, AL, United States

OPEN ACCESS

Edited by:

Maria Tagliamonte,
Istituto Nazionale Tumori Fondazione
G. Pascale (IRCCS), Italy

Reviewed by:

Angela Branche,
University of Rochester, United States
Ciro Leonardo Pierri,
University of Bari Aldo Moro, Italy

*Correspondence:

Mark R. Walter
walter@uab.edu

Specialty section:

This article was submitted to
Viral Immunology,
a section of the journal
Frontiers in Immunology

Received: 06 April 2021

Accepted: 21 May 2021

Published: 04 June 2021

Citation:

Deshpande A, Harris BD,
Martinez-Sobrido L,
Kobie JJ and Walter MR (2021)
Epitope Classification and
RBD Binding Properties of
Neutralizing Antibodies Against
SARS-CoV-2 Variants of Concern.
Front. Immunol. 12:691715.
doi: 10.3389/fimmu.2021.691715

Severe acute respiratory syndrome coronavirus-2 (SAR-CoV-2) causes coronavirus disease 2019 (COVID19) that is responsible for short and long-term disease, as well as death, in susceptible hosts. The receptor binding domain (RBD) of the SARS-CoV-2 Spike (S) protein binds to cell surface angiotensin converting enzyme type-II (ACE2) to initiate viral attachment and ultimately viral pathogenesis. The SARS-CoV-2 S RBD is a major target of neutralizing antibodies (NAbs) that block RBD - ACE2 interactions. In this report, NAb-RBD binding epitopes in the protein databank were classified as C1, C1D, C2, C3, or C4, using a RBD binding profile (BP), based on NAb-specific RBD buried surface area and used to predict the binding epitopes of a series of uncharacterized NAbs. Naturally occurring SARS-CoV-2 RBD sequence variation was also quantified to predict NAb binding sensitivities to the RBD-variants. NAb and ACE2 binding studies confirmed the NAb classifications and determined whether the RBD variants enhanced ACE2 binding to promote viral infectivity, and/or disrupted NAb binding to evade the host immune response. Of 9 single RBD mutants evaluated, K417T, E484K, and N501Y disrupted binding of 65% of the NAbs evaluated, consistent with the assignment of the SARS-CoV-2 P.1 Japan/Brazil strain as a variant of concern (VoC). RBD variants E484K and N501Y exhibited ACE2 binding equivalent to a Wuhan-1 reference SARS-CoV-2 RBD. While slightly less disruptive to NAb binding, L452R enhanced ACE2 binding affinity. Thus, the L452R mutant, associated with the SARS-CoV-2 California VoC (B.1.427/B.1.429-California), has evolved to enhance ACE2 binding, while simultaneously disrupting C1 and C2 NAb classes. The analysis also identified a non-overlapping antibody pair (1213H7 and 1215D1) that bound to all SARS-CoV-2 RBD variants evaluated, representing an excellent therapeutic option for treatment of SARS-CoV-2 WT and VoC strains.

Keywords: SARS-CoV-2, variant of concern, neutralizing antibodies, RBD, ACE2 binding affinity, epitope mapping

INTRODUCTION

A robust humoral immune response to severe acute respiratory syndrome coronavirus-2 (SARS-CoV-2) infection is essential to control viral infection (1, 2). Human neutralizing antibodies (NAbs) that bind to the receptor binding domain (RBD) of the SARS-CoV-2 Spike (S) protein and block ACE2 binding have shown efficacy as therapeutics and are also essential for vaccine efficacy (3–6). The SARS-CoV-2 S protein is a trimer, where the protomers undergo conformational changes essential for viral infectivity (7–10). Specifically, the RBD moves from a “down” conformation, where the ACE2 binding site is buried in the S trimer, to an “up” conformation where the ACE2 binding site is solvent accessible and competent for cell surface ACE2 binding (**Figure 1**). Presumably, the “down” conformation of RBD “hides” the ACE2 binding site in the closed trimeric arrangement to, at least partially, protect the RBD, which is essential for virus cell attachment, from the host’s immune response.

Three-dimensional structural studies have played a large role in our understanding of SARS-CoV-2 S RBD-specific NAb epitopes (**Table 1**). To date, NAbs targeting SARS-CoV-2 RBD have been classified into four structural groups, C1–C4 (**Figure 1**), based on their ability to bind to up or down conformations of the SARS-CoV-2 RBD, and by their overlap with the ACE2 binding site (17). The C1 class is defined by NAbs that bind within the RBD ACE2 binding site, essentially mimicking ACE2 binding, and thus only bind to RBD when it is in the up conformation. The C1 class contains conserved ACE2-blocking NAbs, often composed of heavy chains encoded by the VH3-52 and VH3-66 gene segments (25). C2 NAbs block the ACE2 binding site yet can bind to RBD in its up and down

conformations. C3 NAbs bind largely outside the ACE2 binding site of RBD in both up and down conformations, while a fourth class (C4) binds farther from the ACE2 binding site and the epitope is only accessible once SARS-CoV-2 S undergoes large conformational changes (30). Overall, a variety of NAb/RBD structures have been completed and their interactions defined (see refs. in **Table 1**).

SARS-CoV-2 RBD/NAb structural studies can define NAb mechanisms of action and their potential susceptibility to S protein RBD variants, either alone or in combinations, both of which are observed in VoCs (31–34). Thus, there remains a great need to characterize the molecular details of NAb responses induced upon natural infection and/or by vaccination, at the patient and population levels. This is a large endeavor that ultimately will require protein modeling, combined with synergistic experimental studies and additional 3D structure determinations. As a first step towards this goal, we sought to understand the RBD binding epitopes of a panel of SARS-CoV-2 NAbs, isolated from a single convalescent patient (29). To accomplish this goal, NAb-RBD structures ($n=45$, **Table 1**) in the protein databank (pdb) were grouped into five distinct classes based on their RBD binding profiles. The 17 unknown NAbs (15 from one patient, two from other individuals) were assigned to a NAb/RBD complex and the assignment was validated using RBD variant binding and epitope mapping studies. RBD variants were chosen based on structural considerations and RBD sequence variation observed in the GISAID (35). Of the nine RBD variants tested, N501Y, E484K, and K417T disrupted binding to 65% of the NAbs evaluated. Furthermore, N501Y and E484K RBD variants exhibited essentially wild type (WT) affinity for ACE2, where WT is defined as the Wuhan-1 RBD sequence. Another RBD variant, L452R, disrupted fewer NAbs, but exhibited 2-fold

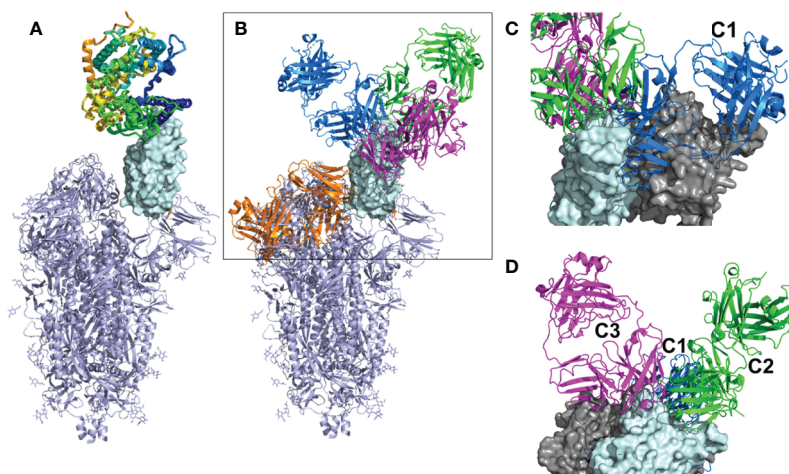


FIGURE 1 | Overall view of ACE2 and NAbs binding to SARS-CoV-2 S protein. **(A)** Ribbon diagram of the SARS-CoV-2 S protein, with one RBD in the up conformation (cyan surface) interacting with ACE2. **(B)** General location of NAb binding epitopes, where an example C1 NAb is colored blue, C2 green, C3 magenta and C4 orange. The figure highlights that extensive conformational changes are required before C4 NAbs can bind to S. **(C)** View of two RBDs from an S trimer (cyan and grey surfaces) in the down conformation, to show that C1 NAbs cannot bind to their epitope while the RBD is in the down conformation, due to steric hindrance. **(D)** Alternative view of adjacent down RBDs in the S trimer showing C2 and C3 NAb epitopes are accessible while RBD is in the down conformation and that some NAbs can bind across an RBD-RBD trimer interface and interfere with RBD opening to bind ACE2.

TABLE 1 | Assignment of Structurally Uncharacterized NAb (unknown) to NAb-RBD Structures in the PDB.

CLASS 1: (n=17)																				
KD (pM)*	IC50 (ng/mL)*	#	pdb	name	unknown	HC BSA	LC BSA	HC of Tot.	HC+LC	M.	Ref.									
186	120/170	1	6xc2	cc12.1	1212F2	766.7	574.9	0.57	1341.6	X	(11)									
		2	6xc4	cc12.3		676.9	186.2	0.78	863.1	X	(11)									
		3	6xe1	CV30		713.5	271.3	0.72	984.8	X	(12)									
		4	7bz5	B38		691.8	501.2	0.58	1193	X	(13)									
11,600	323/204	5	7c01	CB6	736.1	312.6	0.70	1048.7	X	(14)										
738	768/107	6	7cdi	P2C-1F11	1214F4	726.5	229.3	0.76	955.8	X	(15)									
122	210/290				1212D5															
18	1127/168				1214E9															
13,500	460/140				1212D4															
					7							7cjf	–	771	430.8	0.64	1201.8	X	–	
					8							7jmo	COVA2-04	757	369.4	0.67	1126.4	X	(16)	
					9							7k8m	C102	802.4	231	0.78	1033.4	X	(17)	
					10							7kfv	C1A-B12	809.1	375.8	0.68	1184.9	X	(18)	
					11							7kfw	C1A-B3	776.6	371.2	0.68	1147.8	X	(18)	
					12							7kfx	C1A-C2	854.9	353.3	0.71	1208.2	X	(18)	
121	490/380				13							7kfy	C1A-F10	1212D6	797.8	367.8	0.68	1165.6	X	(18)
7.2	900/100													1206D12						
161	240/550	1213F2																		
2,470	872/112	14	7chf	BD-604	712.6	397.2	0.64	1109.8	X	(19)										
		15	7ch5	BD-629	818.2	193.3	0.81	1011.5	X	(19)										
		16	7chb	BD-236	656.3	425	0.61	1081.3	X	(19)										
		17	6xcm	C105	635.2	258.1	0.71	893.3	EM	(17)										
CLASS 1 Distinct (n=5)																				
KD (pM)*	IC50 (ng/mL)*	#	pdb	name	unknown	HC BSA	LC BSA	HC of Tot.	HC+LC	M.	Ref.									
		18	6xkq	CV07-250		422	544.8	0.44	966.8	X	(20)									
		19	6xdg	RGN10933		760.8	187.9	0.80	948.7	X	(4)									
		20	7jx3	S2H14		502.7	408.2	0.55	910.9	X	(21)									
		21	7k9z	298Fab		409.5	302.6	0.58	712.1	X	–									
		22	7jmp	COVA2-39		616.2	143	0.81	759.2	X	(16)									
1,180	66/49				1213H7															
CLASS 2 (n=13)																				
KD (pM)*	IC50 (ng/mL)*	#	pdb	name	unknown	HC BSA	LC BSA	HC of Tot.	HC+LC	M.	Ref.									
21.9	117/85	23	7jv2	S2H13		–	–	–	–	EM										
		24	7k8u	C104		–	–	–	–	EM	(17)									
		25	7k8y	C121	1218A6	741.9	56.4	0.93	798.30	EM	(17)									
9,630	777/1,312	26	7k8s	C002	1206D1	645.2	181.9	0.78	827.10	EM	(17)									
104	10/22-				1212C2															
841	31/26				1212F5															
3,530	300/1,380				1207F10															
					27							7k90	C144	684.9	102.4	0.87	787.30	EM	(17)	
													C144A	693	103.1	0.87	796.10			
													C144AB	1088	118.7	0.90	1206.70			
				C144C	698.4	100.2	0.87	798.60												
		28	6xey	Ab2-4	678.3	160.8	0.81	839.10	EM	(22)										
77	226/59	29	7che	C368-2	600.2	142.5	0.81	742.70	X	(19)										
1,400	210/310	30	7bwj	P2B-2F6	1215D1	481.5	142.6	0.77	624.10	X	(15)									
658	650/180				1207B4															
					1206A5															
					31							7k8w	C119	613.8	346.8	0.64	960.60	EM	(17)	
													C119A	617.3	271.5	0.69	888.80			
													C119B	730.5	34.3	0.96	764.80	EM	(23)	
		32	7byr	Ab23																

(Continued)

TABLE 1 | Continued

CLASS 2 (n=13)											
KD (pM)*	IC50 (ng/mL)*	#	pdb	name	unknown	HC BSA	LC BSA	HC of Tot.	HC+LC	M.	Ref.
2,470	872/112	33	6xkp	CV07-270	1218C8	693.5	106.8	0.87	800.30	X	(20)
		34	7cdj	P2C-1A3		587.5	300.2	0.66	887.70	X	(15)
		35	7k9z	52Fab						X	-
CLASS-3: (n=4)											
KD (pM)*	IC50 (ng/mL)*	#	pdb	common	unknown	HC BSA	LC BSA	HC of Tot.	HC+LC	M.	Ref.
8,150	53/111	36	7k8v	C110A		361	268	-	-	EM	(17)
				C110B		249	320	-	-	EM	(17)
		37	7k8z	C135A		273	135	-	-	EM	(17)
				C135B		354	225	-	-	EM	(17)
				RG10987		512.9	112.7	0.82	625.6	X	(4)
39	7jx3	S309	608.2	167.5	0.78	775.7	X	(24)			
CLASS 4 (n=6)											
KD (pM)*	IC50 (ng/mL)*	#	pdb	common	unknown	HC BSA	LC BSA	HC of Tot.	HC+LC	M.	Ref.
500	>10,000	40	6w41	CR3022		593.4	397.3	0.60	990.7	X	(25)
				EY6A		573	373.4	0.61	946.4	X	(26)
				H014		673.5	287.6	0.70	961.1	EM	(27)
				S2A4		375.5	431.2	0.47	806.7	EM	(21)
				COVA1-16		625.3	153.4	0.80	778.7	X	(28)
				S304		491.3	368.7	0.57	860	X	(21)
				7jx3							
1215B11											

*values taken from reference (29).

LC, light chain; HC, heavy chain; BSA, buried surface area in Å²; M., method; either Xray (X) or electron microscopy (EM), Ref., reference. Common NAb names are bolded if they were used to model of an unknown NAb epitope.

higher affinity for ACE2, suggesting this mutation may enhance viral fitness through increased affinity for ACE2, as well as disrupting the host NAb response. The analysis identified a pair of potent NAb with non-overlapping binding epitopes, 1213H7 (NT₅₀ = 49 ng/mL) and 1215D1 (NT₅₀ = 59 ng/mL), that bound to all nine RBD variants tested. Furthermore, 1215D1 has a novel neutralization mechanism, as it can bind to a preformed RBD-ACE2 complex, potentially allowing it to disrupt the interaction between the virus and ACE2 even after it is formed.

MATERIALS AND METHODS

NAb-RBD Complex Structure Classifications and Assignments

Binary RBD-NAb complex structures (human NAb only), solved by X-ray crystallography and cryo-electron microscopy, were extracted from the pdb (n=45, 12-26-20). RBD surface area buried upon NAb-RBD complex formation was quantified using PISA (36) to define a RBD residue-specific NAb binding profile (BP) for each structure. Buried surface area was not calculated for some complexes (e.g. C104, pdbid = 7k8u), due to almost complete lack of sidechains for the NAb. The NAb BPs were subjected to hierarchical clustering and a correlation-based similarity matrix was calculated using the program Morpheus (<https://software.broadinstitute.org/morpheus>). To evaluate the classifications, RBDs from each NAb-RBD complex were superimposed using the pymol align command

and the resulting NAb classifications were compared visually using pymol (37). Unknown NAb were assigned to the classified NAb by heavy chain sequence alignment using clustal omega (38).

RBD Variant Analysis

SARS-CoV-2 S protein sequences were downloaded from the GISAID (35) for analysis on 1-11-2021. We acknowledge all authors that submitted sequences to the GISAID, which are listed in (<https://www.gisaid.org/>). The RBD region, residues 343-532, of full-length SARS-CoV-2 S sequences (322,688 sequences, **Supplementary Table 1**) were evaluated for amino acid sequence variation at each RBD sequence position, relative to the Wuhan-1 sequence (pubmed accession number NC045512.2) (39). The total number of amino acid changes at each position was counted and converted to a frequency by dividing by the total number of sequences analyzed.

Protein Expression

SARS-CoV-2 NAb were produced and purified as previously described (29). SARS-CoV-2 RBD (Wuhan-1) and RBD variants were produced in insect cells as RBD-FC fusion proteins (29, 40). Briefly, RBD-FC fusion proteins (**Supplementary Figure 1**) were purified from expression media by protein-A affinity chromatography, as previously described (29, 40). Briefly, 6-day transient expressions of RBD-FC WT and variants were performed in drosophila S2 cells. Expression media was incubated with 100uL of protein A beads (Protein A UltraLink, ThermoFisher) for 5 hours on a rotating wheel. The beads were

collected and washed with the 20 column volumes (CV) of 20mM Tris-HCl pH 8, 150mM NaCl and batch eluted with 4CV of 2M Arginine, pH 3.5. The purified RBD-FCs were dialyzed into 20mM Tris-HCl, pH 8, 150mM NaCl and their concentrations quantified by optical density at 280nm. Due to a sequencing error, RBD E484K-FC used for all binding studies was determined to be RBD E484R-FC. Due to the similarity of the amino acid chemistry between Arginine and Lysine, the RBD E484R provides a suitable surrogate for the RBD E484K variant. Soluble ACE2 and RBD-ACE2 fusion protein (RBD-ACE2FP) DNAs were inserted into pMTV5/His and expressed in S2 insect cells as C-terminal his-tagged proteins (Invitrogen). Expression media (100mL) was dialyzed into binding buffer consisting of 20mM Tris HCl, pH 8, 0.5M NaCl, 5mM imidazole (buffer 1). Dialyzed media was incubated with 500uL of nickel affinity beads (his•bind resin, Millipore) that had been charged with 100mM NiSO₄. After 5hrs, the beads were collected, washed with 5CV of buffer 1, followed by 4CV of 20mM Tris HCl, pH 8, 0.5M NaCl, 20mM imidazole. The proteins were batch eluted with 4CV of the same buffer containing 200mM imidazole. The purified proteins were dialyzed against 20mM HEPES, pH 7.4, 150mM NaCl. The concentrations of the purified proteins were determined by optical density at 280nm and used for binding studies.

Surface Plasmon Resonance (SPR) Binding Studies

SPR binding studies were performed using a Biacore T200 (GE life sciences). All studies were performed at 25°C in running buffer consisting of 10mM HEPES, pH 7.4, 150mM NaCl, 0.0075% P20, and 75ug/mL bovine serum albumin. Epitope mapping was performed by capturing RBD-FCs to CM5 sensor chips (Cytiva) using an anti-murine FC capture kit (Cytiva). Two NABs (50nM concentrations) were sequentially injected (NAB1, followed by NAB2) for 90 seconds over each RBD-FC surface, followed by a 60 second dissociation phase. The flowrate for the epitope mapping studies was 30 μ L/min. Binding levels, defined by response units (RU) of each NAB, was recorded following the binding phase of each injection. At the end of each cycle, the surface was regenerated by a 3-minute injection of 10 mM glycine pH 1.7. Competition between NAB epitopes was defined relative to NAB1 [e.g. NAB2 binding (RU)/NAB1 binding (RU)].

ACE2 binding affinity for RBD variants was performed by capturing RBD-FCs to CM5 biacore chips, as described in the epitope mapping studies. Soluble ACE2 was injected over the RBD-FC surfaces at 5 concentrations (300 nM, 75 nM, 18.75 nM, 4.7nM, and 1.2 nM) at a flow rate of 40 μ L/min. The resulting sensorgrams were globally fit to a 1:1 model using Biacore T-200 evaluation software version 1.0 to derive binding constants.

NAB-RBD variant interactions were characterized by injecting RBD-FC Wuhan-1 reference strain, and RBD-FC variants, over NABs captured on CM5 chip surfaces, using a human IgG capture kit (Cytiva). RBD-FCs (50nM) were injected at a flow rate of 50 μ L/min over the NAB surfaces for 90 seconds, followed by a 5 min. dissociation. RBD-variant binding

responses were compared to the RBD reference WT protein (e.g. RU-RBD variant/RU-RBD-WT), collected at the beginning and end of the experiment and converted to percentage of WT binding.

RBD-ACE2FP-NAb epitope analysis was performed injecting RBD-ACE2FP (20nM) over each NAB, coupled as described for the NAB-RBD variant interactions. RBD-ACE2FP was injected over the surface for 90 seconds, followed by a 5 min. dissociation. The flow rate for the experiments was 50 μ L/min. Buffer subtracted sensorgrams were visually evaluated and RU values at 570 seconds, post injection, recorded.

RESULTS

Structure of the RBD-ACE2 Binding Site

The structure of the SARS-CoV-2 RBD-ACE2 complex [(41), PDBID = 6m0j] was used to define RBD residues that bind to ACE2. Residues 333-526 of the 1273 amino acid SARS-CoV-2 S protein form the RBD. The RBD consists of a scaffold, conserved among different coronaviruses, and a variable receptor binding module (RBM), which positions amino acids for contact with ACE2 (42). Three RBM regions: knob (444-449 and 496-505), base (490-494 and 450-456), and tip (473-489), contact the N-terminal α -helical region of ACE2. (**Figures 2A**). A total of 22 RBD residues bury surface area (total = 859Å²) and participate in 15 hydrogen bonds with ACE2, of which 11 are formed by RBD sidechains (**Figures 2B–E**). RBD residues Y449, N487, and Y505 form bivalent hydrogen bonds with ACE2, accounting for 6 of 10 sidechain hydrogen bonds, while K417, Y489, Q493, N498, and T500 form the five remaining sidechain hydrogen bonds with ACE2 (**Figure 2E**). These residues are of particular interest, since RBD amino acid variants in these positions may alter the interaction of RBD with ACE2.

RBD Variant Analysis

As RBD-ACE2 interactions are essential for virus survival, we hypothesized that energetically essential ACE2 binding residues would remain invariant as the virus evolved, while residues less important for ACE2 binding, would be more susceptible to sequence variation. To test this hypothesis, the mutation frequency at each amino acid position in the RBD of SARS-CoV-2 S was compared against the Wuhan-1 reference S RBD sequence (NC045512.2). Of the 322,688 S sequences evaluated, 9 ACE2 binding residues (41%) have remained invariant (0.001% variation or less, **Figure 2E**). These invariant residues cluster within the tip (F456, Y473, N487, Y489) and knob (Y449, G496, Q498, T500, G502) of RBD (**Figures 2A, B**) where they participate in a series of contacts with ACE2 (**Figures 2D, E**). Two invariant residues (Y449 and N487) participate in bivalent hydrogen bonding networks with ACE2, five additional hydrogen bonds are formed with residues Y489, G496, Q498, T500, G502, while F456 and Y473 form a hydrophobic scaffold that allows ACE2 to efficiently pack against the RBD tip (**Figure 2E**). Overall, the invariant residues account for 60% of the hydrogen bonds in the RBD-ACE2 interface. These observations suggest that ACE2 binding requirements restrain

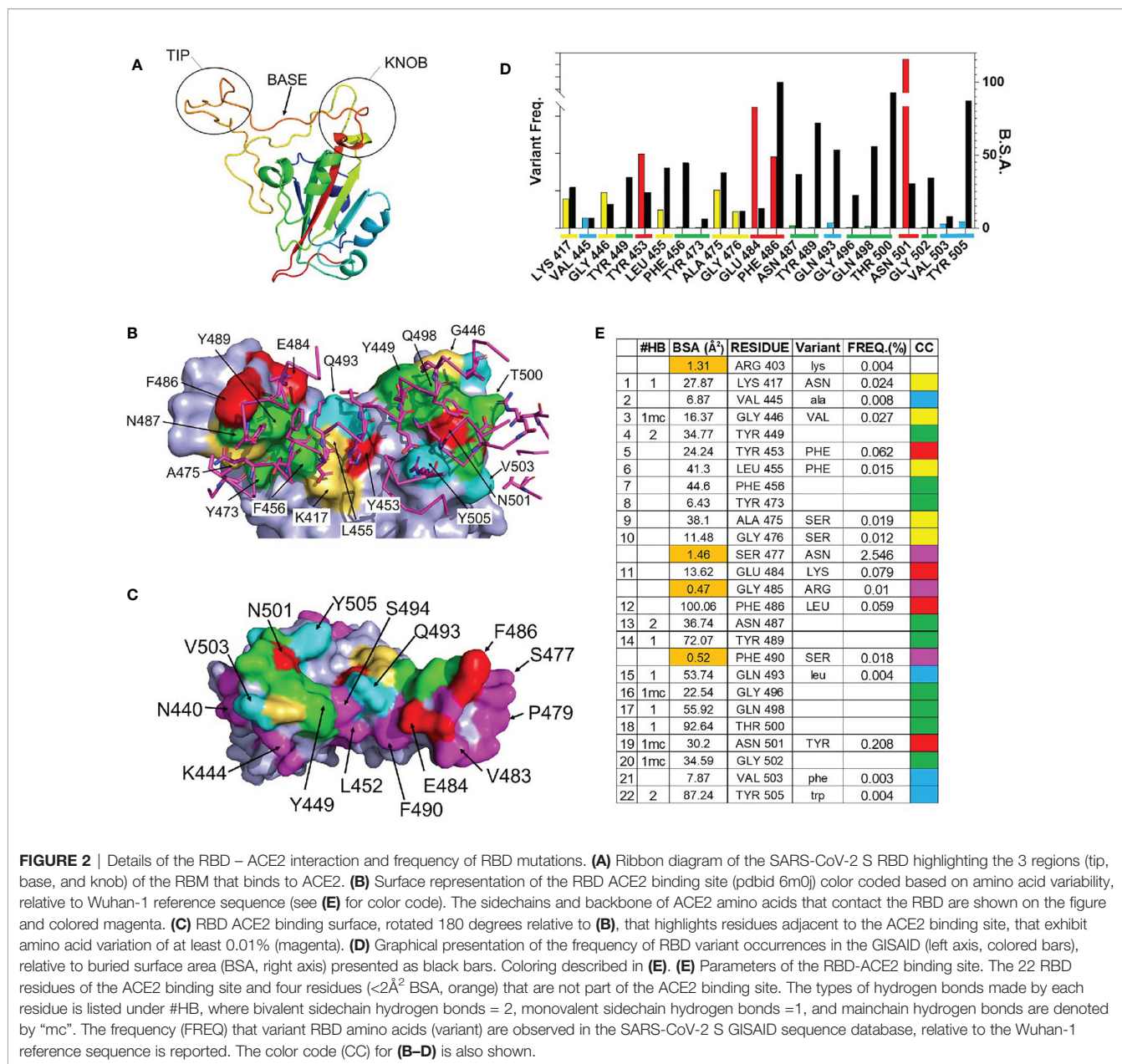


FIGURE 2 | Details of the RBD – ACE2 interaction and frequency of RBD mutations. **(A)** Ribbon diagram of the SARS-CoV-2 S RBD highlighting the 3 regions (tip, base, and knob) of the RBM that binds to ACE2. **(B)** Surface representation of the RBD ACE2 binding site (pdbid 6m0j) color coded based on amino acid variability, relative to Wuhan-1 reference sequence (see **(E)** for color code). The sidechains and backbone of ACE2 amino acids that contact the RBD are shown on the figure and colored magenta. **(C)** RBD ACE2 binding surface, rotated 180 degrees relative to **(B)**, that highlights residues adjacent to the ACE2 binding site, that exhibit amino acid variation of at least 0.01% (magenta). **(D)** Graphical presentation of the frequency of RBD variant occurrences in the GISAID (left axis, colored bars), relative to buried surface area (BSA, right axis) presented as black bars. Coloring described in **(E)**. **(E)** Parameters of the RBD-ACE2 binding site. The 22 RBD residues of the ACE2 binding site and four residues (2\AA^2 BSA, orange) that are not part of the ACE2 binding site. The types of hydrogen bonds made by each residue is listed under #HB, where bivalent sidechain hydrogen bonds = 2, monovalent sidechain hydrogen bonds = 1, and mainchain hydrogen bonds are denoted by "mc". The frequency (FREQ) that variant RBD amino acids (variant) are observed in the SARS-CoV-2 S GISAID sequence database, relative to the Wuhan-1 reference sequence is reported. The color code (CC) for **(B-D)** is also shown.

SARS-CoV-2 RBD amino acid variation at certain positions (**Figures 2D, E**).

In contrast to the invariant residues, 9 ACE2 binding residues (K417, G446, L455, A475, G476, E484, F486, and N501) have undergone significant sequence variation (**Figure 2**) with the largest frequencies occurring at four positions: N501Y (0.208%), E484K (0.079%), Y453F (0.062%), and F486L (0.059%). The N501Y variant, which occurs at the highest frequency, is the only residue located within the RBD knob, while Y453F is located in the RBD base and E484K and F486L are localized in the tip (**Figure 2A**). F486 buries the greatest amount of surface area, of any residue, into the RBD-ACE2 complex. In contrast, Y453, E484, and N501 form limited interactions with ACE2, defined by

lower levels of buried surface area, and only N501 forms a main chain hydrogen bond with ACE2 (**Figure 2**).

Overall, the data show RBD residues that make limited contacts with ACE2 exhibit higher mutation frequencies than those involved in extensive hydrogen bond networks. For example, four SARS-CoV-2 S RBD residues (R403, S477, G485, and F490) bury less than 2\AA^2 of surface area into the complex and do not make hydrogen bonds with ACE2 (**Figure 2D**). Thus, they are near to ACE2 binding residues (**Figure 2C**) yet are not part of the actual ACE2 binding site. Three of these residues, S477 (2.5%), G485 (0.01%), and F490 (0.018%), exhibit high mutation frequencies, showing that significant amino acid variation is more likely for residues that are not essential for

ACE2 binding. Furthermore, the RBD surface diagrams (Figures 2B, C) emphasize that residues exhibiting high mutational frequencies may be located on the edge (e.g. S477) or within (e.g. N501) the ACE2 binding footprint.

NAb/RBD Structures for Classification of NAb RBD Binding Epitopes

Several studies have classified SARS-CoV-2 RBD-binding NABs (17, 43), but an objective clustering rationale, requiring limited investigator interpretation, has not been described. As a result, a database of human NAB/RBD complexes (n=45) was compiled from the protein data bank (pdb) and used to characterize NAb RBD binding epitopes (Table 1). To define distinct features of each NAB/RBD complex, a binding profile (BP) was defined as the RBD residue-specific surface area buried upon NAB/RBD complex formation. NAB BPs were subjected to hierarchical clustering and compared using a similarity matrix (Figure 3). The analysis provided an unbiased classification of anti-RBD NABs into one of 5 distinct groups C1, C1D, C2, C3, and C4. Structures of all NAB/RBD complexes in each class are shown superimposed upon one another in Figure 4 and demonstrate striking structural conservation (e.g. C1) and diversity of NAB epitopes characterized by structural methods.

A total of 17 C1 NABs were found in the pdb. C1 NABs show striking structural conservation of their orientations and RBD-binding epitopes, which overlap substantially with the ACE2

binding site. As a result, C1 NABs only bind to RBD when it is in the “up” conformation in the S protein (Figure 1). BP analysis identified a distinct group of C1-like NABs (C1D, n=5) that do not conserve the orientation or epitope of the C1 class (Figure 4). C1D NABs often bind closer to the flexible RBD tip [e.g. RGN10933 (4)] compared to C1 NABs, which allows them to bind to RBD without it adopting the full “up” conformation required for C1 NABs. Similarly, the steric disruption of C1D NAB COV7-250 binding to RBD in the “down” conformation is minimal (20). Thus, at least some C1D NABs can bind to RBD with only minimal S conformational changes, yet their epitopes still extensively overlap with the ACE2 binding site.

Thirteen examples of C2 NABs were identified, which show even greater diversity in their binding epitopes and orientations than C1 and C1D NABs (Figure 4). In fact, C1, C1D, and C2 NAB epitopes show a progression of binding epitopes and orientations that extend from one side of RBD that forms the ACE2 binding site (e.g. C1 NABs), to the surface opposite the ACE2 binding site, where C2 NABs bind without hindrance to the RBD in either up or down conformations. Thus, the accessibility of the C2 NAB epitopes are greater than for C1 and C1D NABs. As previously reported, the orientations of several C2 NABs, including Ab2-4, C121, and C144, shows they can block adjacent RBDs in the pre-fusion trimer from adopting the “up” ACE2-binding-competent conformations (17, 22).

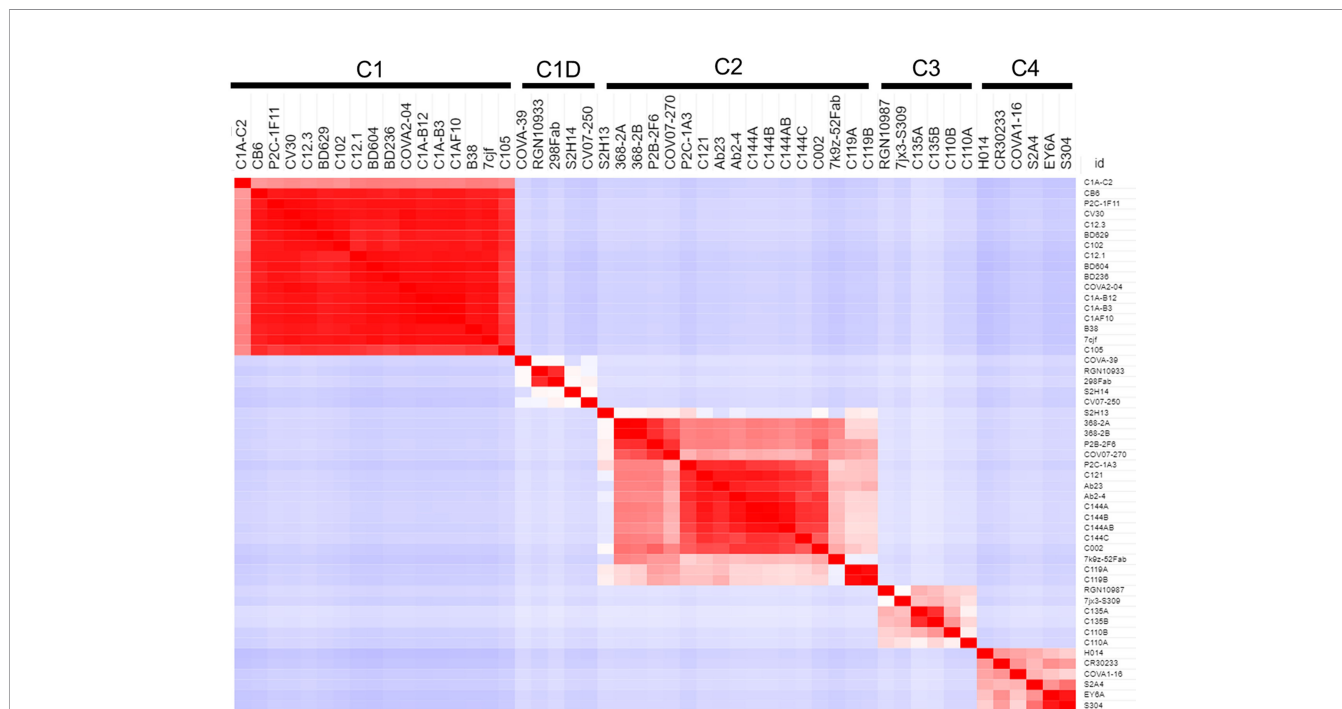


FIGURE 3 | Binding Profile (BP) correlations to define RBD-binding NAb classes. BPs were defined for NAB/RBD complexes (Table 1) that were extracted from the pdb (n=45). For some structures, more than one NAB-RBD complex was evaluated leading to the A, B, C designations for some NABs. Buried surface area was not calculated for some complexes, due to almost complete lack of sidechains for the NABs. The BPs were subjected to hierarchical clustering and then similarity analysis (correlation coefficient calculation) to define five NAB classes C1 (n=17), C1D (n=5), C2 (n=12), C3 (n=4), and C4 (n=6).

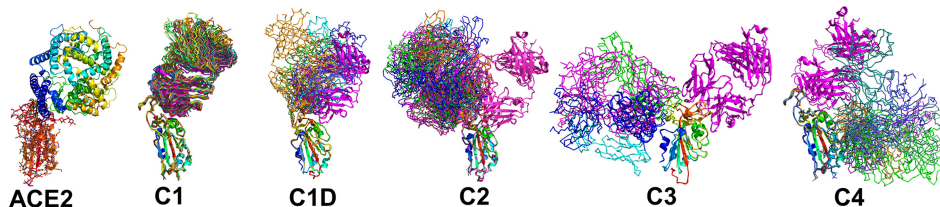


FIGURE 4 | Epitope conservation and diversity within each NAb class. The RBD-ACE2 interaction, as well as all members of each NAb class are shown on the RBD. A ribbon diagram of an archetypical C1 NAb (magenta) is shown in each figure as a structural reference.

The C3 NAb (n=4) binding epitope is localized to the RBD knob and adjacent residues 333-347. C3 NAb adopt distinct orientations, relative to the C1, C1D, and C2 NAb (Figure 4). A unique feature of C3 NAb epitope is its location near RBD-RBD trimer interfaces. As a result, some C3 NAb bind across adjacent RBDs in the trimeric SARS-CoV-2 S and sterically block the RBD up conformation of adjacent RBDs. Some C3 NAb only block the up conformation of the RBD, while others sterically block ACE2 binding, and some have both neutralization mechanisms. Like C2 NAb, C3 NAb epitopes are accessible whether SARS-CoV-2 S RBD is in the up or down conformation. C4 NAb (n=6) bind to an RBD surface comprising a helix-strand-helix motif (residues 366-389) that is buried in the trimeric S, even when the RBD is in the up conformation. Thus, C4 NAb, require SARS-CoV-2 S to undergo significant conformational changes, beyond RBD up-down movements for binding (30). For many C4 NAb, their epitope and orientation prevent them from sterically blocking ACE2 binding. This may explain why many C4 NAb, such as CR3022, do not potently neutralize SARS-CoV-2 compared to NAb in the other classes. However, this is not universal, as the orientations of C4 NAb COVA1-16 and H014 allow them to block ACE2 binding and they are reported to potently neutralize SARS-CoV-2 in cell culture assays and in animal models (27, 28).

Classification of NAb Isolated From a Convalescent SARS-CoV-2 Patient

We previously isolated a series of potent SARS-CoV-2 NAb from a single convalescent patient and characterized their efficacy *in vitro*, and for one NAb (1212C2), its efficacy in golden Syrian hamsters, delivered by inhalation (29). The classified NAb/RBD structures (Table 1 and Figure 4) were used to predict the binding epitopes of these NAb and the resulting assignments were experimentally tested using RBD variant binding and epitope mapping studies. Thus, unknown NAb heavy chains were aligned to the NAb database sequences classified as C1, C1D, C2, C3, or C4 (Figures 3 and 4). Of 20 NAb evaluated, 9 (45%) were classified as C1, 10 (50%) were classified as C2, and one (5%) was classified as C4. The analysis suggested that none of the unknown NAb were C3 NAb, and one of the 20 NAb (1213H7) was misclassified by sequence analysis as a C2 NAb, but subsequently reassigned to the C1D classification based on epitope mapping and RBD variant binding analysis (Figures 5

and 7). Alignments performed with the light chains did not improve the unknown NAb assignments.

Susceptibility of NAb to RBD Variants

The predicted impact of RBD variant residues (Figure 2) on NAb binding was evaluated using the BPs, derived from the NAb/RBD complex structures (Table 1). Variable RBD residues (freq. >0.01) found in at least 75% of the epitopes for each NAb class were identified (Table 2). This analysis identified 11 residues exhibiting increased variability in C1 and C1D NAb epitopes, 7 residues in the C2 epitope, and 2 in C3 NAb epitope. Variable residues that consistently bury surface area in at the C1 NAb class include K417, Y453, L455, A475, F486, and N501. Thus, C1 NAb epitopes are predicted to be sensitive to K417N/T, Y453F, L455F, A475V, F486L, and N501Y variants. Consistent with the structural relationships between C1, C1D, and C2 NAb epitopes (Figure 4), conserved residues within the C1D epitope include residues shared with C1 NAb (e.g. L455, A475, and F486), as well as unique residues E484, and G485. Thus, RBD variants that could disrupt C1D NAb include L455F, A475V, F486L, as well as E484K, and G485R. Contacts conserved across C2 NAb include variable RBD residues G446, L452, V483, E484, F490, and S494. This is consistent with many C2 NAb being sensitive to the E484K variant [(17) and Figure 5]. Additional conserved RBD contacts within the C2 NAb epitope suggests RBD variants G446V, L452R, and S494P can also impact C2 interactions. Based on only four examples, the C3 NAb epitope is diverse and the conserved C3 contact region exhibits limited RBD residue variation. Only two RBD residues in the C3 epitope (N440 and K444) exhibit residue variability greater than 0.01%. Five additional RBD amino acids are contacted by 75% of the C3 NAb, but these amino acid sidechains are highly conserved in the SARS-CoV-2 RBD sequences evaluated. In contrast, amino acid variation within the C1, C1D, and C2 epitopes is much greater (maximal variation 0.12%-2.5%) and extends over more residues. Finally, there are several common contact residues in the C4 NAb epitope, suggesting that N370S, T376I, V382L, P384L, T385I, and R408I could disrupt C4 NAb.

RBD Variant Binding Analysis

Based on the *in silico* NAb epitope analysis, nine RBD variants that localize to the C1 (K417T, A475V, N501Y, Y505W), C1D/

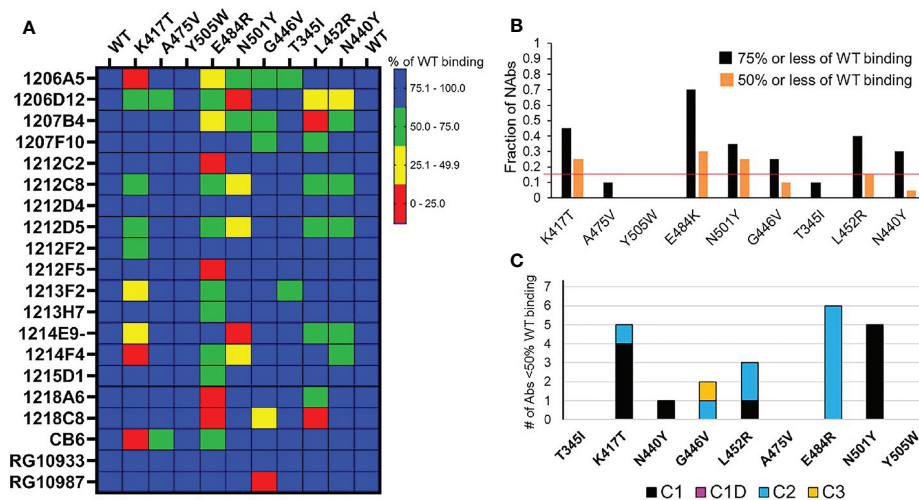


FIGURE 5 | NAb binding to RBD variants. **(A)** SARS-CoV-2 RBD variants were injected over NABs captured on a biacore chip and their binding levels measured and normalized to the binding response to a reference (WT) Wuhan-1 RBD. Two WT RBD binding experiments were performed at the beginning and end of the experiment to validate the reproducibility of the assay. NAB binding is presented in the matrix as % of WT binding. **(B)** Global summary of NAB binding to SARS-CoV-2 RBD variants. Black bars show the fraction of NABs that exhibit red, yellow, or green levels of binding as shown in **(A)**. Orange bars represent the fraction of NABs that exhibit red and yellow binding, as shown in **(A)**. The horizontal red line highlights the RBD variants (K417T, E484K, and N501Y) that disrupt the binding of the largest number of NABs. **(C)** Sensitivity of NAB classes to the different RBD variants. The number of NABs that display less than 50% of WT binding in **(A)** (red and yellow boxes) were counted (y axis) and plotted according to their NAB classification (**Table 1**).

C2 (G446V, L452R and E484K) and C3 epitopes (T345I, N440Y, and G446V) were produced for binding studies with the unknown NABs. C4 NABs were excluded from the analysis. Our structural analysis, and recent literature (17), confirm that the loss of NAB binding to certain SARS-CoV-2 RBD variants can be used to identify NAB classes. Furthermore, the assays can be used to identify NABs that are not sensitive to RBD variants and thus potentially useful as therapeutics. To address these questions, the unknown NABs and three controls [CB6 (14), RGN10933 and RGN10987 (4)] were tested for their ability to bind to the SARS-CoV-2 RBD variants (**Figure 5**). NAB-RBD interactions were defined as “significantly disrupted” if NAB binding to an RBD variant was reduced by 50% or more, relative to the reference WT RBD. Based on this definition, C1 RBD variants K417T (25%) and N501Y (25%), and C2 variant E484K (30%), most frequently disrupted NAB binding (**Figure 5**). A second group of RBD variants, L452R (15%), G446V (10%), and N440Y (5%) disrupted fewer NAB interactions, while all NABs bound efficiently (>50%, relative to WT reference) to RBD variants T345I, A475V, and Y505W. Efficient binding of all NABs to T345I (freq. = 0.0003%) and Y505W (freq. = 0.004%) is consistent with their high conservation within the SARS-CoV-2 RBD (**Table 2**). Furthermore, for those NABs exhibiting >50% reduction in binding levels, relative to WT RBD, E484K and N501Y exclusively disrupted NABs classified as C2 and C1, respectively (**Figure 5C**).

ACE2-RBD Variant Binding Analysis

In addition to disrupting NAB binding, SARS-CoV-2 RBD mutations can impact RBD-ACE2 binding affinity, which could

impact virus infectivity. Thus, ACE2 binding affinity was measured for each RBD variant and the reference Wuhan-1 RBD protein (**Figure 6**). The two RBD variants that disrupted the largest number of NAB interactions (E484K, and N501Y) bound to ACE2 within 15% (e.g. error of the measurements) of the WT RBD-ACE2 interaction. In contrast, K417T, which disrupts a salt bridge with ACE2 (**Figure 2B**), exhibited two-fold lower binding affinity for ACE2, relative to WT RBD (**Figure 6B**). This data suggests 2 of the 3 most disruptive RBD mutations are NAB evading mutations that do not alter interactions with the viral receptor, ACE2. T345I and N440Y also exhibited WT RBD-ACE2 binding affinity, while G446V and A475V exhibited disrupted ACE2 binding affinities, like K417T. Two RBD mutations (L452R and Y505W) exhibited higher affinity for ACE2 than WT RBD. Thus, L452R disrupts several NABs, but also binds to ACE2 with higher affinity. Thus, the L452R mutant, associated with a recently identified California VoC (B.1.427/B.1.429-California) has evolved to enhance ACE2 binding while simultaneously disrupting a significant number of NABs in the C2 classification. Y505W also enhances RBD-ACE2 interactions but was not disruptive to any of the NABs tested (**Figure 5A**).

NAB Epitope Analysis

Epitope mapping was performed to further validate the assignment of the NABs to the different classes. Based on their 50% neutralization (NT_{50}) values and RBD variant binding properties, 12 NABs were subjected to epitope mapping analysis (**Figure 7**). Overall, there was excellent correlation between the NAB assignments (**Table 1**) and the epitope analysis. For example, C1 vs. C1 NABs, or other “like-like” classifications prevented

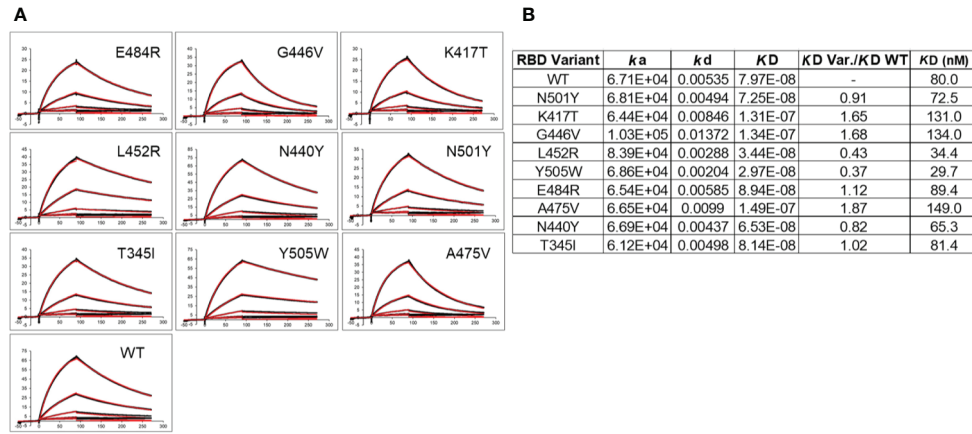


FIGURE 6 | ACE2 binding to SARS-CoV-2 S RBD variants. **(A)** Sensorgrams of RBD variants binding to ACE2. Black lines correspond to the experimental sensorgram data and the red lines correspond to the calculated sensorgrams used to define the binding constants. Units of the x and y axes of each sensorgram are seconds and response units (RU), respectively. **(B)** Binding constants derived from the sensorgrams.

binding of the second NAb. In contrast, some C1 NAb allowed simultaneous binding of a second C2 NAb, but this was not universal. For example, C1 NAb 1212D5, 1212F2, 1213F2, 1212D4, and 1212C8, allowed simultaneous binding of C2 NAb 1207B4, 1215D1, and 1207F10 (**Figure 7**). In contrast, the C2 NAb 1212C2 blocked all C1 and C2 NAb that were assayed (**Figure 7A**). To address these observations, structures of the NAb-RBD complexes assigned to the different C2 NAb were compared (**Figure 7D**). Specifically, 1215D1, 1207B4, and

1207F10 NAb were assigned to the C386-2/RBD complex, while 1212C2 was assigned to the C121/RBD complex. As shown in **Figure 7D**, 1212C2 (modeled by C121-RBD) overlaps with C1 (modeled by P2C-1F11/RBD) and C2 NAb, while 1215D1 (modeled by C386-2/RBD) can simultaneously bind with several C1 (1214D4, 1212C8, 1212D5 etc.) and C1D (1213H7) NAb. Thus, the assignment of each NAb to a NAb/RBD complex provided a structural basis for understanding the overlapping and distinct epitopes of the unknown NAb

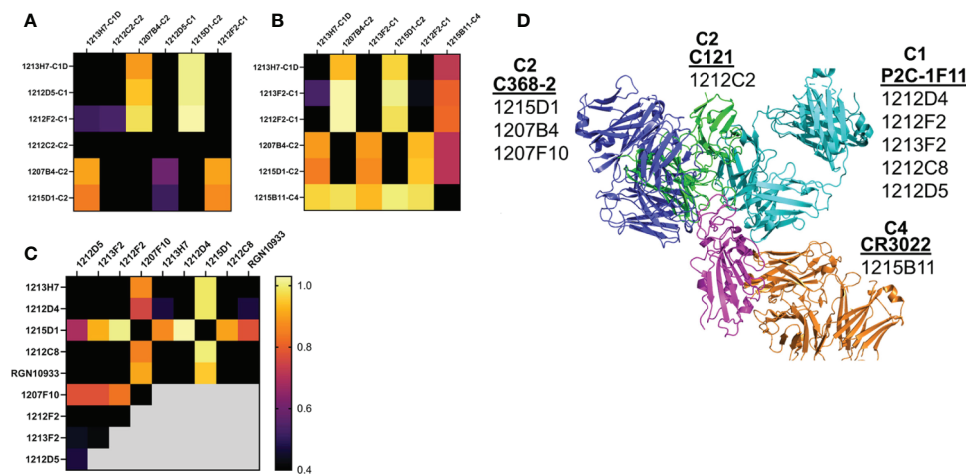


FIGURE 7 | NAb epitope mapping. SPR-based epitope mapping performed to further validate the classification of unknown NAb assigned to an NAb/RBD complex (**Table 1**). **(A-C)** represent 3 distinct mapping experiments performed with common and distinct NAb, showing NAb/RBD complexes that were assigned to the unknown NAb and used to explain the epitope mapping data. P2C-1F11/RBD was used to model C1 NAb, C2 NAb were modeled by C386-2/RBD (1215D1, 1207B4 and 1207F10) and C121/RBD (1212C2) structures, while the C4 NAb, 1215D11, was modeled by the RBD/CR3022 structure. The assigned structures explain how 1212C2 epitope blocks all other NAb from binding to RBD, while 1212D4 (or 1213H7) and 1215D1 bind to non-overlapping RBD epitopes and also bind to all RBD variants they were tested against (**Figure 5**). Two NAb evaluated in the mapping data (1213H7 and c1l RGN10933) are not listed on the graphical summary. 1213H7 and RGN10933 were both assigned as C1D NAb, which is consistent with their common epitope mapping profiles, and their ability to bind simultaneously with 1215D1.

TABLE 2 | SARS-CoV-2 RBD residues conserved in ≥75% of NAb epitopes and the frequencies of variants.

	C1	Avg. BSA	% Cons.	Variant	Freq.		C1D	Avg. BSA	% Cons.	Variant	Freq.
1	Y505	97.2	100	W:	0.004%	1	F486	152.3	100	L	0.059%
2	K417	80.2	100	N	0.024%	2	Y489	77.9	100	–	–
3	F486	61.6	100	L	0.059%	3	Q493	60.7	100	K	0.004%
4	F456	57.1	100	–	–	4	E484	54.1	100	K	0.079%
5	Y489	50.9	94	–	–	5	F456	48.7	100	–	–
6	R403	50.9	100	I	0.004%	6	Y449	40.5	80	–	–
7	A475	49.1	100	S	0.019%	7	N487	35.7	100	H	0.001%
8	Y421	48.0	100	–	–	8	L455	34.0	100	F	0.015%
9	K458	45.1	100	M	0.001%	9	S477	33.2	80	N	2.546%
10	Q493	41.0	100	K	0.004%	10	A475	33.0	100	V	0.012%
11	L455	39.4	94	F	0.015%	11	G485	27.4	100	R	0.010%
12	N487	37.2	100	H	0.001%	12	Q498	26.7	80	–	–
13	T415	33.1	94	M	0.001%	13	T478	19.1	80	I	0.063%
14	Q498	31.6	88	–	–	14	K417	17.8	80	N	0.024%
15	G502	28.6	100	–	–	15	G476	14.7	80	S	0.012%
16	Y473	27.5	94	–	–	16	Y453	11.3	100	F	0.062%
17	Y453	27.3	100	F	0.062%	17	S494	5.0	80	P	0.046%
18	N460	26.3	100	H	0.002%						
19	N501	25.0	100	Y	0.208%						
20	G476	24.0	100	S	0.012%						
21	G416	21.4	100	–	–						
22	S477	20.5	100	N	2.546%						
23	T500	19.5	88	–	–						
24	D420	17.8	94	–	–						
25	D405	15.2	94	–	–						
26	Y495	13.1	88	–	–						
27	S459	11.2	100	F	0.021%						
28	R457	10.7	100	–	–						
29	G496	10.2	76	–	–						
30	S494	8.7	88	P	0.046%						
31	Q474	8.7	100	–	–						
32	F490	7.5	76	S	0.018%						

	C2	Avg. BSA	% Cons.	Variant	Freq.		C3	Avg. BSA	% Cons.	Variant	Freq.
1	Y449	88.8	100	–	–	1	R346	69.2	100	K	0.009%
2	E484	85.1	100	K	0.079%	2	T345	61.9	75	–	–
3	F490	53.6	92	S	0.018%	3	L441	44.6	100	–	–
4	Q493	39.1	92	K	0.004%	4	N440	40.9	75	K	0.016%
5	V483	29.0	92	A	0.020%	5	K444	24.9	75	R	0.010%
6	G446	24.9	92	V	0.027%	6	N450	18.3	75	–	–
7	S494	23.1	92	P	0.046%	7	N448	15.4	75	–	–
8	L452	22.5	92	R	0.121%						
9	G485	20.4	83	R	0.010%						
10	L492	8.0	100	–	–						

Red highlights frequencies > 0.01%.

RBD variants shown in bold lettering were evaluated for NAb and ACE2 binding.

As a second method of epitope analysis, the NABs were tested for their ability to bind to an RBD-ACE2 fusion protein (FP). The RBD-ACE2FP was designed to provide a stable RBD-ACE2 complex to characterize the overlap of NAb epitopes with the RBD-ACE2 binding site. As expected, most NABs bound very poorly to the RBD-ACE2FP, consistent with their epitope being blocked by ACE2 (Figure 8). However, three C2-classified NABs (1215D1, 1207B4, and 1207F10) exhibited high levels of binding to the RBD-ACE2FP (Figure 8). Based on the location of the RBD ACE2 binding site (Figure 4), this data further validates the assignment of these NABs to the C2 class (Figure 7D). It also suggests that this subclass of C2 NABs may disrupt RBD-ACE2 interactions even after the complex is formed, presumably by a conformational change, providing a novel mechanism of neutralization for this group of C2 NABs.

DISCUSSION

The goal of this study was to use SARS-CoV-2 NAb/RBD structural information found in the protein databank and SARS-CoV-2 S RBD sequence variation data from the GISAID, to characterize a series of NABs for potential use as therapeutics against SARS-CoV-2. Optimal NABs against SARS-CoV-2 have always required that they exhibit high potency neutralizing capabilities, but as the pandemic has continued, they now must also exhibit broad specificity against naturally occurring SARS-CoV-2 VoC. The current VoC include B.1.1.7-UK (N501Y, S494P*, E484K*), P.1-Japan/Brazil (K417N/T, E484K, N501Y), B.1.351-South Africa (K417N, E484K, N501Y) B.1.427/B.1.429-California

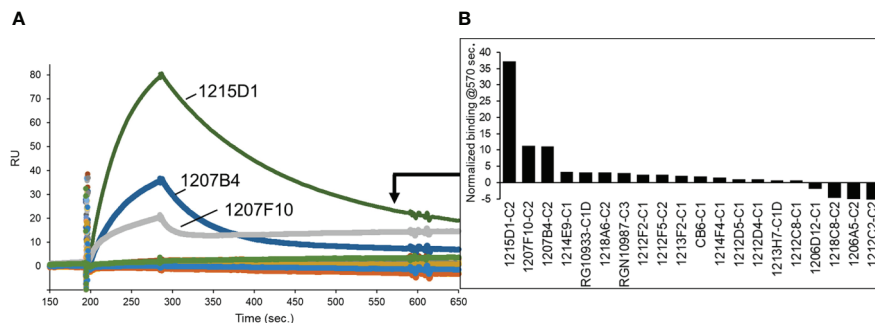


FIGURE 8 | NAb epitope analysis using a SARS-CoV-2 RBD-ACE2 fusion protein. **(A)** NABs were captured on anti-IgG biacore chips and sensorgrams were recorded for an RBD-ACE2 fusion protein (20nM) injected over the surface of each NAb. **(B)** Variability in fusion protein binding levels near the end of the sensorgrams ($t = 570$ seconds) is plotted in the graph.

(L452R), where amino acid changes in the SARS-CoV-2 S RBD of these VoC are listed in parentheses (44).

RBD amino acid mutations found in the VoC, with the exception of the K417T mutation (K417T frequency = 0 in the analysis on 1-11-21), are found in the top 20 of most frequently observed mutations (frequency > 0.024%) in the GISAID. SARS-CoV-2 VoC have been shown to reduce Ab-mediated neutralization and/or exhibit increased disease severity and transmissibility (44–46). To further evaluate these single mutations at the molecular level, we tested a panel of SARS-CoV-2 NABs, isolated from a convalescent patient, for their ability to bind to a series of SARS-CoV-2 RBD variants. The analysis found that E484K is the most disruptive mutation and impacted the greatest number of NABs tested in our study (30%), with N501Y and K417T being slightly less disruptive, but still each impacting 25% of the NABs evaluated. Combined, the 3 SARS-CoV-2 RBD variants (K417T, E484K, and N501Y) present in the P.1 Japan/Brazil and B.1.351 South Africa VoC significantly disrupted the binding of 65% of the NABs tested.

In addition to disrupting NAb binding, which is correlated with reduced virus neutralization, the impact of the variants on ACE2 binding affinity was determined. This is an important question, often not addressed, that may define mechanisms of viral selection responsible for increased infectivity and/or disease severity, as well as disrupting host NAb responses. Analysis of RBD-variant/ACE2 binding affinity revealed that N501Y and E484K exhibited essentially WT affinity for ACE2, where WT corresponds to the Wuhan-1 SARS-CoV-2 RBD sequence. RBD variants N440Y and T345I also exhibited ACE2 binding affinity similar to WT RBD. This suggests that neither N501Y and/or E484K variants increase infectivity, reported for the B.1.1.7 UK VoC, by increasing affinity for ACE2. If increased ACE2 affinity is required for increasing viral infectivity, other mutations in the SARS-CoV-2 S, such as D614G, P681H, or several other changes, alone or together, must be responsible for enhanced ACE2 binding affinity. Overall, our data suggests that N501Y and E484K (For E484K, this is inferred from the evaluation of the E484R mutation in our studies), enhance viral fitness

predominantly by disrupting the host NAb response, but not by increasing ACE2 binding affinity.

Like N501Y and E484K, K417T also significantly disrupts NAb binding. However, the K417T variant, as well as the G446V and A475V variants exhibit reduced (~2-fold) ACE2 binding affinity. Thus, escape from NAb binding/neutralization at these positions comes with a cost of reducing ACE2 binding affinity, suggesting these mutants are unlikely to confer a selective advantage to the virus though enhanced viral attachment. In contrast, L452R exhibited a 2-fold increase in ACE2 affinity. This is consistent with the B.1.429 California VoC being able to evade NAb responses, as well as enhance ACE2 binding affinity, possibly providing advantages in immune evasion against NABs, and increased cell infectivity *via* enhanced ACE2 binding affinity, ultimately leading to increased disease severity. A weakness in our studies is that our RBD-ACE2 binding analysis studies are based on a 1:1 monomeric ACE2-RBD interaction. It is possible that the conformation and function of the RBD variants are distinct in the context of the trimeric SARS-CoV-2 S. Recent data suggests that the D614G mutation stabilizes the S trimer and is necessary to observe the functional impact of the N501Y and L452R mutations on cell infectivity (47, 48). It is also possible that large changes in RBD-ACE2 affinity, higher or lower, disrupts optimal viral infectivity, while more subtle changes around the reference WT RBD-ACE2 binding affinity can cause large changes in cell infectivity.

From an overall analysis of SARS-CoV-2 anti-RBD NABs, C3 NABs appear to have an advantage by targeting an RBD epitope that has undergone less variation than NAb epitopes associated with C1, C1D, and C2 NABs. However, variability in CDR length, structure, and amino acid composition has thus far been sufficient for at least some C1, C1D, and C2 NABs to maintain their neutralization efficacy, despite RBD variability. Furthermore, we find the C3 RGN10987 NAB is highly sensitive to the G446V variant, suggesting the virus has identified RBD variant residues that disrupt the binding of NABs from each NAB class. For the unknown NABs evaluated

in this report, the NAb/RBD database, RBD variant binding studies, and epitope mapping allowed their assignment into specific NAb classes. Thus, our study provides a strategy for characterizing NAb/RBD epitopes at a larger scale to further define NAb sensitivity to RBD variants in individuals recovered from natural infections and changes in the anti-RBD SARS-CoV-2 structural repertoire induced by vaccination. Finally, our analysis identified a non-overlapping antibody pair, 1213H7/1215D1, which both bind to all RBD variants found in current SARS-CoV-2 VoC, suggesting they represent a potential therapeutic treatment for SARS-CoV-2 WT and newly identified VoC.

DATA AVAILABILITY STATEMENT

The original contributions presented in the study are included in the article/**Supplementary Material**. Further inquiries can be directed to the corresponding author.

ETHICS STATEMENT

AD, LM-S, JJK, and MRW are co-inventors on a patent for NAbS described in the study.

REFERENCES

- Ni L, Ye F, Cheng ML, Feng Y, Deng YQ, Zhao H, et al. Detection of SARS-CoV-2-Specific Humoral and Cellular Immunity in COVID-19 Convalescent Individuals. *Immunity* (2020) 52:971–977.E973. doi: 10.1016/j.immuni.2020.04.023
- McAndrews KM, Dowlatshahi DP, Dai J, Becker LM, Hensel J, Snowden LM, et al. Heterogeneous Antibodies Against SARS-CoV-2 Spike Receptor Binding Domain and Nucleocapsid With Implications for COVID-19 Immunity. *JCI Insight* (2020) 5:2379–3708. doi: 10.1172/jci.insight.142386
- Walsh EE, Frenck RW Jr., Falsey AR, Kitchin N, Absalon J, Gurtman A, et al. Safety and Immunogenicity of Two RNA-Based Covid-19 Vaccine Candidates. *New Engl J Med* (2020) 383:2439–50. doi: 10.1056/NEJMoa2027906
- Hansen J, Baum A, Pascal KE, Russo V, Giordano S, Wloga E, et al. Studies in Humanized Mice and Convalescent Humans Yield a SARS-CoV-2 Antibody Cocktail. *Sci (N Y NY)* (2020). doi: 10.1126/science.abd0827
- Rogers TF, Zhao F, Huang D, Beutler N, Burns A, He WT, et al. Isolation of Potent SARS-CoV-2 Neutralizing Antibodies and Protection From Disease in a Small Animal Model. *Sci (N Y NY)* (2020). doi: 10.1126/science.abc7520
- Baum A, Ajithdoss D, Copin R, Zhou A, Lanza K, Negron N, et al. Regn-COV2 Antibodies Prevent and Treat SARS-CoV-2 Infection in Rhesus Macaques and Hamsters. *Sci (N Y NY)* (2020) 370:1110–5. doi: 10.1126/science.abe2402
- Walls AC, Park YJ, Tortorici MA, Wall A, McGuire AT, Veesler D. Structure, Function, and Antigenicity of the SARS-CoV-2 Spike Glycoprotein. *Cell* (2020) 181:281–92.e286. doi: 10.1016/j.cell.2020.02.058
- Wrapp D, Wang N, Corbett KS, Goldsmith JA, Hsieh C-L, Abiona O, et al. Cryo-EM Structure of the 2019-nCoV Spike in the Prefusion Conformation. *Sci (N Y NY)* (2020) 367:1260–3. doi: 10.1126/science.abb2507
- Turoňová B, Sikora M, Schürmann C, Hagen WJH, Welsch S, Blanc FEC, et al. In Situ Structural Analysis of SARS-CoV-2 Spike Reveals Flexibility Mediated by Three Hinges. *Sci (N Y NY)* (2020) 370:203–8. doi: 10.1101/2020.06.26.173476
- Mercurio I, Tragni V, Busto F, De Grassi A, Pierri CL. Protein Structure Analysis of the Interactions Between SARS-CoV-2 Spike Protein and the Human ACE2 Receptor: From Conformational Changes to Novel

AUTHOR CONTRIBUTIONS

MRW and AD conceived the study. AD, BDH, and MRW performed experiments. AD, MRW, LM-S, and JJK wrote and edited the paper. All authors contributed to the article and approved the submitted version.

FUNDING

UAB internal funds were used for this study.

ACKNOWLEDGMENTS

We acknowledge use of the UAB Heflin Genomics Core, UAB Multidisciplinary Molecular Interaction Core Facility.

SUPPLEMENTARY MATERIAL

The Supplementary Material for this article can be found online at: <https://www.frontiersin.org/articles/10.3389/fimmu.2021.691715/full#supplementary-material>

- Neutralizing Antibodies. *Cell Mol Life Sci: CMLS* (2021) 78:1501–22. doi: 10.1007/s00018-020-03580-1
- Yuan M, Liu H, Wu NC, Lee CD, Zhu X, Zhao F, et al. Structural Basis of a Shared Antibody Response to SARS-Cov-2. *Sci (N Y NY)* (2020) 369:1119–23. doi: 10.1126/science.abd2321
 - Hurlburt NK, Seydoux E, Wan YH, Edara VV, Stuart AB, Feng J, et al. Structural Basis for Potent Neutralization of SARS-CoV-2 and Role of Antibody Affinity Maturation. *Nat Commun* (2020) 11:5413. doi: 10.1038/s41467-020-19231-9
 - Wu Y, Wang F, Shen C, Peng W, Li D, Zhao C, et al. A Noncompeting Pair of Human Neutralizing Antibodies Block COVID-19 Virus Binding to Its Receptor ACE2. *Sci (N Y NY)* (2020) 368:1274–8. doi: 10.1126/science.abc2241
 - Shi R, Shan C, Duan X, Chen Z, Liu P, Song J, et al. A Human Neutralizing Antibody Targets the Receptor-Binding Site of SARS-CoV-2. *Nature* (2020) 584(7819):120–4. doi: 10.1038/s41586-020-2381-y
 - Ju B, Zhang Q, Ge J, Wang R, Sun J, Ge X, et al. Human Neutralizing Antibodies Elicited by SARS-CoV-2 Infection. *Nature* (2020) 584(7819):115–9. doi: 10.1101/2020.03.21.990770
 - Wu NC, Yuan M, Liu H, Lee CD, Zhu X, Bangaru S, et al. An Alternative Binding Mode of IGHV3-53 Antibodies to the SARS-CoV-2 Receptor Binding Domain. *Cell Rep* (2020) 33:108274. doi: 10.1016/j.celrep.2020.108274
 - Barnes CO, Jette CA, Abernathy ME, Dam KA, Esswein SR, Gristick HB, et al. Sars-CoV-2 Neutralizing Antibody Structures Inform Therapeutic Strategies. *Nature* (2020) 588:682–7. doi: 10.1038/s41586-020-2852-1
 - Clark SA, Clark LE, Pan J, Coscia A, McKay LGA, Shankar S, et al. Sars-CoV-2 Evolution in an Immunocompromised Host Reveals Shared Neutralization Escape Mechanisms. *Cell* (2021). doi: 10.1016/j.cell.2021.03.027
 - Du S, Cao Y, Zhu Q, Yu P, Qi F, Wang G, et al. Structurally Resolved SARS-CoV-2 Antibody Shows High Efficacy in Severely Infected Hamsters and Provides a Potent Cocktail Pairing Strategy. *Cell* (2020) 183:1013–23.e1013. doi: 10.1016/j.cell.2020.09.035
 - Kreye J, Reincke SM, Kornau HC, Sánchez-Sendin E, Corman VM, Liu H, et al. A Therapeutic non-Self-Reactive SARS-CoV-2 Antibody Protects From Lung Pathology in a COVID-19 Hamster Model. *Cell* (2020) 183:1058–69.e1019. doi: 10.1016/j.cell.2020.09.049

21. Piccoli L, Park YJ, Tortorici MA, Czudnochowski N, Walls AC, Beltramello M, et al. Mapping Neutralizing and Immunodominant Sites on the SARS-CoV-2 Spike Receptor-Binding Domain by Structure-Guided High-Resolution Serology. *Cell* (2020) 183:1024–42.e1021. doi: 10.1016/j.cell.2020.09.037
22. Liu L, Wang P, Nair MS, Yu J, Rapp M, Wang Q, et al. Potent Neutralizing Antibodies Against Multiple Epitopes on SARS-CoV-2 Spike. *Nature* (2020) 584:450–6. doi: 10.1038/s41586-020-2571-7
23. Cao Y, Su B, Guo X, Sun W, Deng Y, Bao L, et al. Potent Neutralizing Antibodies Against SARS-CoV-2 Identified by High-Throughput Single-Cell Sequencing of Convalescent Patients' B Cells. *Cell* (2020) 182:73–84.e16. doi: 10.1016/j.cell.2020.05.025
24. Pinto D, Park YJ, Beltramello M, Walls AC, Tortorici MA, Bianchi S, et al. Cross-Neutralization of SARS-CoV-2 by a Human Monoclonal SARS-CoV Antibody. *Nature* (2020) 583:290–5. doi: 10.1038/s41586-020-2349-y
25. Yuan M, Wu NC, Zhu X, Lee CD, So RTY, Lv H, et al. A Highly Conserved Cryptic Epitope in the Receptor Binding Domains of SARS-CoV-2 and SARS-CoV. *Sci (N Y NY)* (2020) 368:630–3. doi: 10.1126/science.abb7269
26. Zhou D, Duyvesteyn HME, Chen CP, Huang CG, Chen TH, Shih SR, et al. Structural Basis for the Neutralization of SARS-CoV-2 by an Antibody From a Convalescent Patient. *Nat Struct Mol Biol* (2020) 27:950–8. doi: 10.1038/s41594-020-0480-y
27. Lv Z, Deng YQ, Ye Q, Cao L, Sun CY, Fan C, et al. Structural Basis for Neutralization of SARS-CoV-2 and SARS-CoV by a Potent Therapeutic Antibody. *Sci (N Y NY)* (2020) 369:1505–9. doi: 10.1126/science.abc5881
28. Liu H, Wu NC, Yuan M, Bangaru S, Torres JL, Caniels TG, et al. Cross-Neutralization of a SARS-CoV-2 Antibody to a Functionally Conserved Site is Mediated by Avidity. *Immunity* (2020) 53:1272–80.e1275. doi: 10.1016/j.immuni.2020.10.023
29. Piepenbrink MS, Park JG, Oladunni FS, Deshpande A, Basu M, Sarkar S, et al. Therapeutic Activity of an Inhaled Potent SARS-CoV-2 Neutralizing Human Monoclonal Antibody in Hamsters. *Cell Rep Med* (2021) 2:100218. doi: 10.1016/j.xcrm.2021.100218
30. Huo J, Zhao Y, Ren J, Zhou D, Duyvesteyn HME, Ginn HM, et al. Neutralization of SARS-CoV-2 by Destruction of the Prefusion Spike. *Cell Host Microbe* (2020) 28:445–54.e446. doi: 10.1016/j.chom.2020.06.010
31. Wang Z, Schmidt F, Weisblum Y, Muecksch F, Barnes CO, Finkin S, et al. mRNA Vaccine-Elicited Antibodies to SARS-CoV-2 and Circulating Variants. *Nature* (2021). doi: 10.3410/f.739524179.793585051
32. Liu Z, VanBlargan LA, Bloyet LM, Rothlauf PW, Chen RE, Stumpf S, et al. Identification of SARS-CoV-2 Spike Mutations That Attenuate Monoclonal and Serum Antibody Neutralization. *Cell Host Microbe* (2021) 29:477–88.e474. doi: 10.1016/j.chom.2021.01.014
33. Baum A, Fulton BO, Wloga E, Copin R, Pascal KE, Russo V, et al. Antibody Cocktail to SARS-CoV-2 Spike Protein Prevents Rapid Mutational Escape Seen With Individual Antibodies. *Sci (N Y NY)* (2020) 369(6506):1014–8. doi: 10.1126/science.abd0831
34. Greaney AJ, Starr TN, Gilchuk P, Zost SJ, Binshtein E, Loes AN, et al. Complete Mapping of Mutations to the SARS-CoV-2 Spike Receptor-Binding Domain That Escape Antibody Recognition. *Cell Host Microbe* (2021) 29:44–57.e49. doi: 10.1016/j.chom.2020.11.007
35. Elbe S, Buckland-Merrett G. Data, Disease and Diplomacy: GISAID's Innovative Contribution to Global Health. *Global Challenges* (2017) 1:33–46. doi: 10.1002/gch2.1018
36. Krissinel E, Henrick K. Inference of Macromolecular Assemblies From Crystalline State. *J Mol Biol* (2007) 372:774–97. doi: 10.1016/j.jmb.2007.05.022
37. DeLano WL. *The PyMOL Molecular Graphics System DeLano Scientific*. San Carlos, CA, USA (2002). Available at: <http://www.pymol.org>.
38. Madeira F, Park YM, Lee J, Buso N, Gur T, Madhusoodanan N, et al. The EMBL-EBI Search and Sequence Analysis Tools APIs in 2019. *Nucleic Acids Res* (2019) 47:W636–41. doi: 10.1093/nar/gkz268
39. Wu F, Zhao S, Yu B, Chen YM, Wang W, Song ZG, et al. A New Coronavirus Associated With Human Respiratory Disease in China. *Nature* (2020) 579:265–9. doi: 10.1038/s41586-020-2008-3
40. Deshpande A, Putcha BD, Kuruganti S, Walter MR. Kinetic Analysis of Cytokine-Mediated Receptor Assembly Using Engineered FC Heterodimers. *Protein Sci* (2013) 22:1100–8. doi: 10.1002/pro.2285
41. Lan J, Ge J, Yu J, Shan S, Zhou H, Fan S, et al. Structure of the SARS-CoV-2 Spike Receptor-Binding Domain Bound to the ACE2 Receptor. *Nature* (2020) 581:215–20. doi: 10.1038/s41586-020-2180-5
42. Li F, Li W, Farzan M, Harrison SC. Structure of SARS Coronavirus Spike Receptor-Binding Domain Complexed With Receptor. *Sci (N Y NY)* (2005) 309:1864–8. doi: 10.1126/science.1116480
43. Yuan M, Liu H, Wu NC, Wilson IA. Recognition of the SARS-CoV-2 Receptor Binding Domain by Neutralizing Antibodies. *Biochem Biophys Res Commun* (2021) 538:192–203. doi: 10.1016/j.bbrc.2020.10.012
44. Du S, Cao Y, Zhu Q, Yu P, Qi F, Wang G, et al. Structurally Resolved SARS-CoV-2 Antibody Shows High Efficacy in Severely Infected Hamsters and Provides a Potent Cocktail Pairing Strategy. *Cell* (2020) 183:1013–23.e1013.
45. Davies NG, Abbott S, Barnard RC, Jarvis CI, Kucharski AJ, Munday JD, et al. Estimated Transmissibility and Impact of SARS-CoV-2 Lineage B.1.1.7 in England. *Sci (N Y NY)* (2021) 372:eabg3055. doi: 10.1126/science.abg3055
46. Tegally H, Wilkinson E, Giovanetti M, Iranzadeh A, Fonseca V, Giandhari J, et al. Emergence and Rapid Spread of a New Severe Acute Respiratory Syndrome-Related Coronavirus 2 (SARS-CoV-2) Lineage With Multiple Spike Mutations in South Africa. *MedRxiv: Preprint Server Health Sci* (2020) 2012.2021.20248640. doi: 10.1101/2020.12.21.20248640
47. Deng X, Garcia-Knight MA, Khalid MM, Servellita V, Wang C, Morris MK, et al. Transmission, Infectivity, and Antibody Neutralization of an Emerging SARS-CoV-2 Variant in California Carrying a L452R Spike Protein Mutation. *MedRxiv: Preprint Server Health Sci* (2021). doi: 10.1101/2021.03.07.21252647
48. Zhang L, Jackson CB, Mou H, Ojha A, Peng H, Quinlan BD, et al. Sars-CoV-2 Spike-Protein D614G Mutation Increases Virion Spike Density and Infectivity. *Nat Commun* (2020) 11:6013. doi: 10.1038/s41467-020-19808-4

Conflict of Interest: The authors declare that the research was conducted in the absence of any commercial or financial relationships that could be construed as a potential conflict of interest.

Copyright © 2021 Deshpande, Harris, Martinez-Sobrido, Kobie and Walter. This is an open-access article distributed under the terms of the Creative Commons Attribution License (CC BY). The use, distribution or reproduction in other forums is permitted, provided the original author(s) and the copyright owner(s) are credited and that the original publication in this journal is cited, in accordance with accepted academic practice. No use, distribution or reproduction is permitted which does not comply with these terms.